MEASUREMENTS AND IMPACT OF STRAY FIELDS ON THE 380 GeV DESIGN OF CLIC

C. Gohil[1][†], P.N. Burrows, JAI, University of Oxford, Oxford, United Kingdom
E. Marin, D. Schulte, M. Buzio, CERN, Geneva, Switzerland
[1]also at CERN, Geneva, Switzerland

Abstract

Previous studies of the 3 TeV Compact Linear Collider (CLIC) design have shown a sensitivity to external dynamic magnetic fields (stray fields) on the nanoTesla level [1]. In this paper the obtained tolerances for stray fields in the 380 GeV CLIC design are presented. In order to determine potential stray field sources, a measurement sensor has been acquired and used to investigate the magnetic contamination from technical equipment. The collected measurements, as well as details of the sensor, are discussed.

INTRODUCTION

The Compact Linear Collider (CLIC) is an e^+e^- linear collider proposed for the CERN site. The implementation will take place in three centre-of-mass energy (E_{CM}) stages. A first stage at $E_{CM} = 380$ GeV will permit precise physics studies of the Higgs and $t\bar{t}$ threshold. This will be followed by an intermediate energy stage, assumed to be $E_{CM} = 1.5$ TeV, depending on the physics requirements. And finally, the full capacity of CLIC will be exploited at $E_{CM} = 3$ TeV [2].

Previous studies on the impact of external dynamic magnetic fields (stray fields) on the 3 TeV CLIC design found a tolerance on the order of one nT to remain within a 2% luminosity loss budget [1]. The sensitivity of the 380 GeV CLIC design is presented in this paper.

A schematic diagram of the 380 GeV CLIC design is shown in Fig. 1. This study focuses on three sections of CLIC: the long transfer line in the Ring to Main Linac (RTML), which transports the beam from the Damping Rings to the Main Linac; the Main Linac (ML) and the Beam Delivery System (BDS).
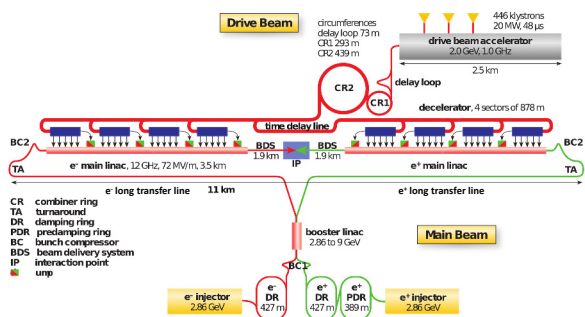
Figure 1: Layout of the 380 GeV CLIC design [3].

† chetan.gohil@cern.ch

STRAY FIELD TOLERANCES

Simulations used to calculate tolerances were performed with the particle tracking code PLACET [4]. To simulate the stray fields a grid of dipole kickers was placed in the beam-line with a spacing of 0.1 m. The strength of each dipole was set to represent a vertical kick from a sinusoidal stray field oriented in the horizontal plane. The wavelength of the stray field was varied and the vertical emittance growth recorded. The tolerance was calculated as the stray field amplitude that results in a 1.2 nm normalised vertical emittance growth (equivalent to a 2% luminosity loss).

The effect of a stray field is to coherently kick the beam so that it develops an offset and angle. This offset (y) and angle (y') leads to an emittance growth through filamentation, which at a waist is given by

$$\Delta\epsilon_y = \frac{1}{2}\frac{y^2}{\sigma_y^2} + \frac{1}{2}\frac{y'^2}{\sigma_{y'}^2}, \tag{1}$$

where σ_y is the beam size and $\sigma_{y'}$ is the beam divergence.

Two different types of stray fields were considered: symmetric and anti-symmetric fields about the interaction point (IP). For anti-symmetric fields, the colliding beams are kicked in opposite directions and the luminosity loss is dominated by an offset at collision. However, for symmetric fields, the beams are kicked in the same direction. This means there is no offset at collision and the luminosity loss is dominated by an emittance growth due to the stray field.
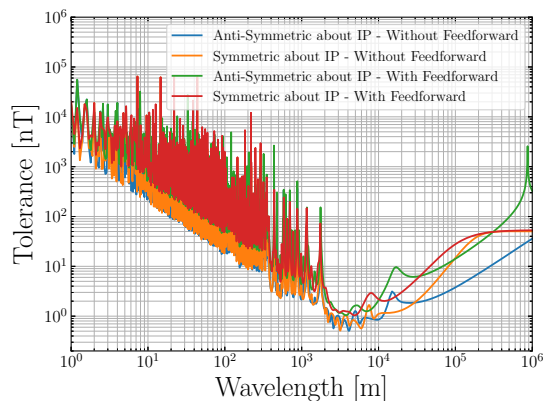
Figure 2: Tolerance versus stray field wavelength in the RTML transfer line for a 1.2 nm vertical emittance growth, with and without a feedforward correction in the turn-around.

The tolerance for a stray field in the RTML transfer line is shown in Fig. 2. There is a sensitivity at 3 km, which corresponds to the stray field wavelength approaching the betatron wavelength. In comparison with the 3 TeV design,

the shorter transfer line is less sensitive to stray fields by a factor of the length ratio squared.

The RTML contains a turn-around (TA in Fig. 1) near the end of the section. This provides the possibility of a feedforward orbit correction. Figure 2 shows the stray field tolerance (in green and red) with a feedforward mechanism that fully corrects the orbit in the turn-around and without a feedforward correction (in blue and orange). The feedforward correction significantly reduces the sensitivity.
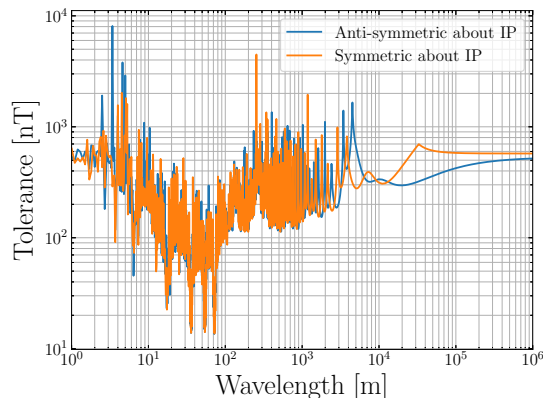
Figure 3: Tolerance versus stray field wavelength in the ML for a 1.2 nm vertical emittance growth.

The tolerance for a stray field in the ML is shown in Fig. 3. In comparison with the 3 TeV design, the ML is less sensitive to stray fields, with tolerances on the order of 1 nT reported in [1].
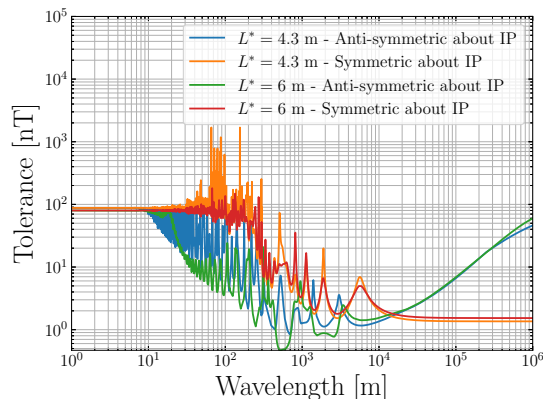
Figure 4: Tolerance versus stray field wavelength in the $L^* = 4.3$ m and $L^* = 6$ m BDS designs for a 1.2 nm vertical emittance growth.

Stray field tolerances were calculated for two different BDS designs. These designs differ in the distance (L^*) between the final quadrupole and IP. Figure 4 shows the stray field tolerance for $L^* = 4.3$ m (in blue and orange) and $L^* = 6$ m (in green and red). The 380 GeV BDS shows a similar sensitivity compared to the 3 TeV design, with tolerances on the order of 1 nT reported in [1].

There is a fine structure that is apparent in Figs. 2-4. This arises from the offset and angle in Eq. (1) being dependent on the the Twiss parameters (α_y, β_y), phase advance ($\Delta\phi_y$), beam energy (γ_r) and strength of the dipole kick (δ) as shown in Eqs. (2) and (3).

$$y(s_2) = \sqrt{\frac{\beta_y(s_1)\beta_y(s_2)\gamma_r(s_1)}{\gamma_r(s_2)}} \sin(\Delta\phi_y(s_1, s_2))\delta(s_1) \quad (2)$$

$$y'(s_2) = \sqrt{\frac{\beta_y(s_1)\gamma_r(s_1)}{\beta_y(s_2)\gamma_r(s_2)}}\{\cos(\Delta\phi_y(s_1, s_2)) \\ - \alpha_y(s_2)\sin(\Delta\phi_y(s_1, s_2))\}\delta(s_1) \quad (3)$$

where s_1 is the location of the kick and s_2 is the end of a section. The dipole kicks themselves are a sine or cosine function depending on the symmetry.

STRAY FIELD SOURCES

Sources of stray fields can be classified as man-made or natural. Natural sources, such as the Earth's magnetic field, typically produce stray fields of frequencies less than 1 Hz. Such stray fields can be effectively mitigated with the use of a beam-based orbit correction. Stray fields from natural sources with frequencies greater than 1 Hz occur infrequently (less than once a month) and are typically within the tolerance [5].

For CLIC, man-made sources can either be an environmental source, which is a piece of equipment that produces a stray field, but is not an element of CLIC, or a technical source, which is an element of CLIC. Examples of environmental sources are the electrical grid and railways. CLIC operates with a repetition rate of 50 Hz, i.e. the same frequency as the electrical grid. This means that stray fields from the electrical grid appear static and can be removed by tuning. Other running accelerators can also act as an environmental source, particularly on the CERN site where there are several other running experiments.

Technical sources, such as RF systems, vacuum pumps and power cables, pose the greatest risk. A technical source that is discussed in [1], which is specific to CLIC is the drive beam. Technical sources are capable of producing stray fields across a wide frequency range. However, the beam pipe will provide shielding against stray fields of very high frequency. A 2 mm copper coating will reduce stray fields of frequency 1 kHz or greater by a factor of $1/e$ or more.

To study the impact of stray fields on CLIC, realistic measurements of their power spectra are essential. These power spectrums are expected to be dependent on the local geology and environment, therefore, measurements on the CERN site are required. In 2017, the background magnetic field on the CERN site was measured to a sub-nT precision [6]. These measurements were done with a single fluxgate magnetometer with a frequency range of 0-20 Hz. However, this was not enough to measure the full spectrum due to the limited frequency range of the sensor. In this paper further measurements over a wider frequency range in the CERN Linear Electron Accelerator for Research (CLEAR) facility on the Meyrin, CERN site are presented, as well as measurements in the Large Hadron Collider (LHC) tunnel and in the ALICE detector cavern.

05 Beam Dynamics and EM Fields

D01 Beam Optics - Lattices, Correction Schemes, Transport

MEASUREMENTS

Measurements of stray fields were performed with a one-axis induction coil magnetometer, the LEMI-144 produced by the Lviv Centre of Institute of Space Research [7], and a three-axis fluxgate magnetometer, the Mag-03 produced by Bartington Instruments [8]. These sensors were used with a 16-bit National Instruments USB-6366 DAQ [9]. The specifications are summarised in Table 1.

Table 1: LEMI-144 [7] and Mag-03 [8] specifications.

Technical Parameter	LEMI-144	Mag-03
Frequency bandwidth	0.1-300 Hz	0-3 kHz
Noise level (at 1 Hz)	0.6 pT/√Hz	6 pT/√Hz
Resolution (16-bit DAQ)	8 pT	31 nT
Magnetic field range	±250 nT	±1 mT

Figure 5 shows the stray field simultaneously recorded by the LEMI-144 and Mag-03 in the vertical direction (radially outward from the Earth) on the 15th March, 2018. This measurement was taken without the CLEAR accelerator running in order to measure the background magnetic field. A regular pattern was observed, which was correlated to the pulsing of the dipole magnets in the Proton Synchrotron (PS) ring, located approximately 80 m away. The largest magnetic field fluctuations were approximately 100 nT in amplitude and occurred with a frequency of less than 1 Hz.
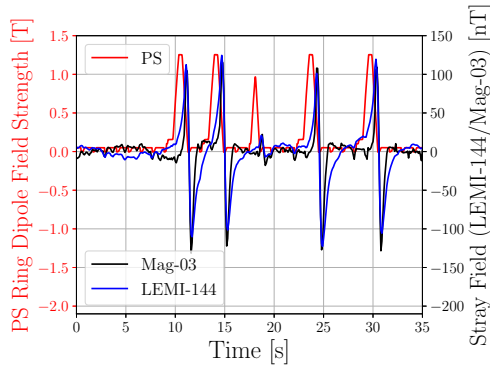
Figure 5: Background magnetic field variation measurement at the CLEAR facility on the 15th March, 2018. The Mag-03 signal was filtered for the frequency range 0.1-300 Hz.

This pulsing was observed in the previous measurement campaign, where magnetic field variations of approximately 70 nT were observed at a distance of 90 m from the PS ring. These measurements show an attenuation that scales with the distance from the ring cubed, which is the expected far-field behaviour of a dipole. In the absence of any shielding material, a distance of approximately 370 m from the PS ring would diminish the signal to sub-nT levels.

Figure 6 shows the power spectral density of background magnetic field variations recorded in the LHC tunnel (in red) and in the ALICE detector cavern (in orange). These measurements were taken with the LEMI-144 at a time where the LHC was not in operation. There is a significantly larger

power spectral density in the cavern compared to the LHC tunnel. This highlights that the detector can act as a significant technical source.
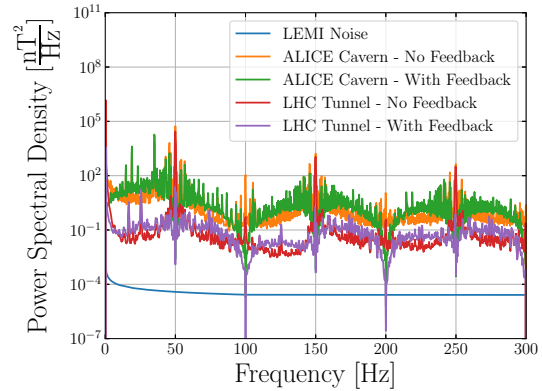
Figure 6: Average power spectral density of the background magnetic field measured at 8 different locations in the LHC tunnel and ALICE detector cavern on the 31st January, 2018.

The effect of a perfect orbit correction with a dead-beat feedback system of unity gain is also shown in Fig. 6. Although the harmonics of 50 Hz are mostly cured, with a reduction by a factor of 100 at 50 Hz in the LHC tunnel, the influence of the stray field is amplified in regions in between.

It can be seen from Fig. 6 that the floor of the power spectral density remains relatively constant with increasing frequency, suggesting a signal exists at higher frequencies. A sensor with a wider frequency bandwidth is required in order to obtain the full spectrum.

CONCLUSIONS

Measurements taken to date characterise the background magnetic field. A more realistic power spectrum for CLIC would be one in the vicinity of a running accelerator. However, this puts requirements on the radiation hardness of the sensor. Neither the LEMI-144 nor the Mag-03 is radiation hard so they cannot be used in a live accelerator environment.

To fully understand the impact of stray fields, the spatial distribution must also be measured. With this, a two dimensional power spectral density can be determined. This type of measurement requires multiple sensors measuring simultaneously. The acquisition of further sensors is planned.

Due to the tight tolerances, mitigation methods will be essential for CLIC. Some mitigation techniques were discussed in [1] for the 3 TeV design. These methods can also be applied to the 380 GeV design. Most likely a combination of active systems, such as beam-based orbit correction systems, and passive systems, such as metallic coating of beam pipes, will be required. In the design of an active system, the frequency dependence of the stray fields must be known. Figure 6 highlights that a simple orbit correction can potentially amplify the problem. For this, further measurements to characterise stray fields on the CERN site are planned.

05 Beam Dynamics and EM Fields

D01 Beam Optics - Lattices, Correction Schemes, Transport

REFERENCES

[1] J. Snuverink *et al.*, "Impact of Dynamic Magnetic Fields on the CLIC Main Beam", in *Proc. IPAC'10*, Kyoto, Japan, May 2010.

[2] M. Aicheler *et al.*, "A Multi-TeV Linear Collider Based on CLIC Technology CLIC Conceptual Design Report", CERN, Geneva, Switzerland, Rep. CERN-2012-007, Oct. 2012.

[3] P.N. Burrows *et al.*, "Updated baseline for a staged Compact Linear Collider", CERN, Geneva, Switzerland, Rep. CERN-2016-004, Aug. 2016.

[4] A. Latina *et al.*, "Recent Improvements of the Tracking Code PLACET", in *Proc. EPAC'08*, June 2008.

[5] C. Beggan, Mini-Workshop on Impact of Stray Fields on Accelerators, CERN, Geneva, Switzerland, Oct. 2017.

[6] E. Marin *et al.*, "Impact of Dynamical Stray Fields on CLIC", in *Proc. IPAC'17*, May 2017.

[7] *Induction Coil Magnetometer LEMI-144 User Manual*, Lviv Centre of Institute of Space Research, Lviv, Ukraine, 2017.

[8] *Operational Manual for Mag-03 Three-Axis Magnetic Field Sensors*, Bartington Instruments Limited, Oxford, England, 2018.

[9] *X Series User Manual*, National Instruments Corporation, Austin, USA, 2018.